Molecular Self-Assembly of Mixed High-Beta Zwitterionic and Neutral Ground-State NLO Chromophores

Michael Halter,[†] Yi Liao,[†] Ryan M. Plocinik,[‡] David C. Coffey,[§] Sanchali Bhattacharjee,[†] Ursula Mazur,[△] Garth J. Simpson,[‡] Bruce H. Robinson,[†] and Sarah L. Keller*[,†]

Departments of Chemistry and Physics, University of Washington, Seattle, Washington 98195, Department of Chemistry, Purdue University, West Lafayette, Indiana 47907, and Chemistry and Materials Science Program, Washington State University, Pullman, Washington 99164

Received August 10, 2007. Revised Manuscript Received December 5, 2007

We investigate a strategy for producing organic NLO materials with high chromophore densities by assembling Langmuir monolayers and Langmuir–Blodgett films containing mixtures of two hyperpolarizable chromophore amphiphiles. When deposited at an air–water interface, the amphiphilic molecules are oriented with their molecular hyperpolarizabilities aligned, and their dipole moments antialigned. We find that mixed chromophore Langmuir monolayers are more stable than pure ones, suggesting that electrostatic interactions aid self-assembly and ordering. Upon transfer of the monolayers to glass and silicon substrates, aggregates with well-defined topological features appear. We characterize aggregate formation using fluorescence microscopy, atomic force microscopy, and nonlinear optical ellipsometry, and we propose a mechanism for aggregate formation. Understanding molecular interactions between strong chromophores should enable fabrication strategies that prevent aggregation and optimize chromophore alignment. Overall, our results suggest that electrostatic forces can be successfully applied to the assembly of the chromophores within bulk nonlinear optical materials containing densely packed, highly ordered, mixed chromophore systems.

Introduction

Nanoscale assembly of chromophores with high dipole moments and strong hyperpolarizabilities has resulted in photonic devices with impressive performance characteristics.[1–4] For rodlike chromophores (i.e., with molecular tensors dominated by interactions along a single internal coordinate), the nonlinear optical (NLO) activity of a material increases with the hyperpolarizability, concentration, and ordering of its constituent chromophores. One method for aligning chromophores in a polymer matrix is to apply an electric field near the polymer's glass transition temperature, and then cool the polymer before removing the field. This method of electric field poling is less successful at high chromophore concentrations because intermolecular electrostatic interactions tend to antialign dipoles of neighboring chromophores, resulting in centrosymmetric structures and decreased bulk NLO activity.[5–7]

Here we describe a method for producing organic NLO materials with high chromophore density and alignment through the assembly of monolayer films containing two different chromophore types (Figure 1). Our approach is designed to eliminate electrostatic effects that result from using only one type of chromophore. Our fabrication strategy introduces amphiphilic chromophores with positive and negative hyperpolarizabilities ($+\beta$ and $-\beta$) as shown in Figure 1. For the $-\beta$ chromophore, the primary component of the first order hyperpolarizability is in the opposite direction from the ground-state dipole moment.[8–13] An amphiphile is made from the $-\beta$ chromophore by conjugating an alkyl chain to the electron accepting group. The $+\beta$ chromophore is complementary, with an alkyl chain conjugated to the electron donating moiety.

We have assembled mixtures of $+\beta$ and $-\beta$ chromophore amphiphiles on a Langmuir trough such that dipole coupling between chromophores enhances rather than diminishes chromophore ordering at high chromophore concentrations (Figure 1). Our goal is to use layer-by-layer nanoscale assembly techniques to produce films of mixed $+\beta$ and $-\beta$ chromophores in which intermolecular dipole interactions

* Corresponding author. Fax: (206) 685-8665. E-mail: slkeller@chem.washington.edu.
[†] Department of Chemistry, University of Washington.
[‡] Purdue University.
[§] Department of Physics, University of Washington.
[△] Washington State University.

(1) Dalton, L. R.; Steier, W. H.; Robinson, B. H.; Zhang, C.; Ren, A.; Garner, S.; Chen, A. T.; Londergan, T.; Irwin, L.; Carlson, B.; Fifield, L.; Phelan, G.; Kincaid, C.; Amend, J.; Jen, A. *J. Mater. Chem.* **1999**, *9* (9), 1905–1920.
(2) Kajzar, F.; Lee, K. S.; Jen, A. K. Y. Polymeric Materials and Their Orientation Techniques for Second-Order Nonlinear Optics. In *Polymers for Photonics Applications II*; Springer: New York, 2003; Vol. 161 pp 1−85.
(3) Shi, Y. Q.; Zhang, C.; Zhang, H.; Bechtel, J. H.; Dalton, L. R.; Robinson, B. H.; Steier, W. H. *Science* **2000**, *288* (5463), 119–122.
(4) Dalton, L. R.; Robinson, B. H.; Jen, A. K. Y.; Steier, W. H.; Nielsen, R. *Opt. Mater.* **2003**, *21* (1–3), 19–28.
(5) Dalton, L. R.; Harper, A. W.; Robinson, B. H. *Proc. Natl. Acad. Sci. U. S. A.* **1997**, *94* (10), 4842–4847.
(6) Robinson, B. H.; Dalton, L. R. *J. Phys. Chem. A* **2000**, *104* (20), 4785–4795.
(7) Sullivan, P. A.; Rommel, H.; Liao, Y.; Olbricht, B. C.; Akelaitis, A. J. P.; Firestone, K. A.; Kang, J. W.; Luo, J.; Davies, J. A.; Choi, D. H.; Eichinger, B. E.; Reid, P. J.; Chen, A.; Jen, A. K. Y.; Robinson, B. H.; Dalton, L. R. *J. Am. Chem. Soc.* **2007**, *129* (24), 7523–7530.

10.1021/cm702267z CCC: $40.75
Published on Web 02/05/2008

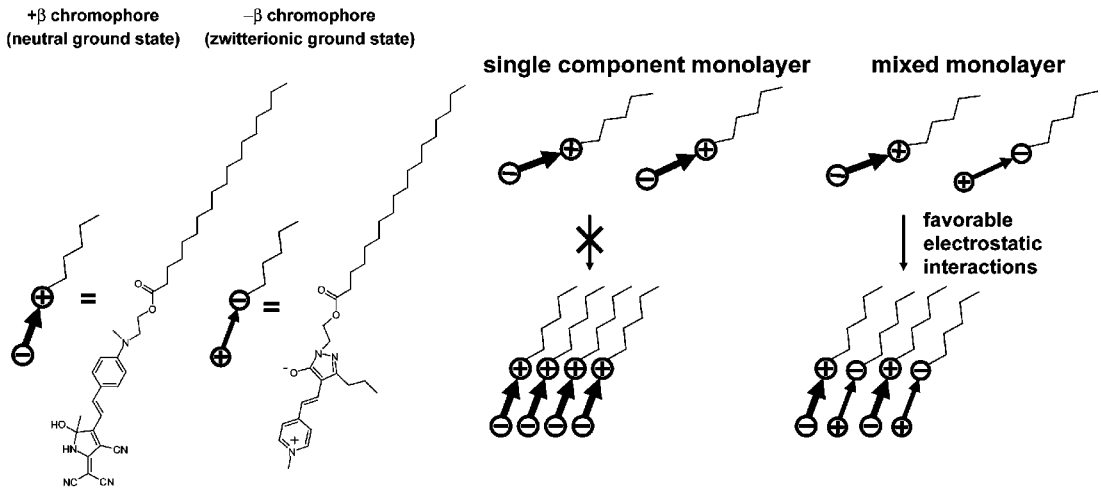

Figure 1. Left: Molecular structures of the $+\beta$ neutral ground-state amphiphilic chromophore and the $-\beta$ zwitterionic ground-state amphiphilic chromophore. Right: Arrows indicate the direction of the primary component of the first molecular hyperpolarizability of chromophore amphiphiles assembled on a Langmuir trough. The molecular dipole moment of each amphiphilic chromophore is indicated by + and − signs, and the attached acyl chains are drawn above each chromophore. Electrostatic interactions between dipole moments that have an antiparallel alignment stabilize high density mixed $+\beta$ and $-\beta$ chromophore monolayers.

promote favorable molecular ordering for optimal bulk NLO activity. To the best of our knowledge, this is the first application of the $+\beta$ and -β chromophores in Langmuir−Blodgett (LB) films. One other previous attempt to overcome disruptive electrostatic interactions between neighboring chromophores utilized an anionic surfactant mixed with a cationic amphiphilic chromophore.[14] The attractive electrostatic interactions within these mixed films resulted in an improvement in the chromophore ordering and second harmonic generation. Another strategy that has been used successfully to improve the optical activity of LB films is the application of amphiphilic bis-chromophores.[15] In this work, two covalently attached chromophores of the same sign were used to generate homogeneous and stable films with high chromophore densities. In addition to LB film deposition, layer-by-layer assembly techniques such as sequential synthesis using siloxane chemistry,[16–21] trifunctional silane chemistry,[22–24] and zirconium phosphate/phosphonate chemistry[25–27] could be used to generate the mixed chromophore films described here.

We investigate the miscibility and self-assembly of mixed $+\beta$ and $-\beta$ chromophores in Langmuir monolayers and in Langmuir–Blodgett transferred films using fluorescence microscopy, atomic force microscopy (AFM), and nonlinear optical ellipsometry. We find that mixed $+\beta$ and $-\beta$ chromophore monolayers at the air/water interface are significantly more stable than monolayers of either chromophore alone. Once transferred to substrates, temperature-dependent molecular rearrangements occur, illustrating problems inherent in constructing photonic devices containing chromophores with strong dipole moments.[4–6,28,29] We propose a consistent mechanism for our observations on the basis of multiple characterization techniques. Not only are assembly strategies for constructing highly ordered NLO films technologically valuable but understanding chromophore intermolecular interactions is also useful for designing poled-polymer films.

(8) Bell, N. A.; Bradley, C. S.; Broughton, R. A.; Coles, S. J.; Hibbs, D. E.; Hursthouse, M. B.; Ray, A. K.; Simmonds, D. J.; Thorpe, S. C. *J. Mater. Chem.* **2005**, *15* (14), 1437–1445.
(9) Kay, A. J.; Woolhouse, A. D.; Gainsford, G. J.; Haskell, T. G.; Barnes, T. H.; McKinnie, I. T.; Wyss, C. P. *J. Mater. Chem.* **2001**, *11* (4), 996–1002.
(10) Kay, A. J.; Woolhouse, A. D.; Zhao, Y. X.; Clays, K. *J. Mater. Chem.* **2004**, *14* (8), 1321–1330.
(11) Marder, S. R.; Beratan, D. N.; Cheng, L. T. *Science* **1991**, *252* (5002), 103–106.
(12) Marder, S. R.; Cheng, L. T.; Tiemann, B. G.; Friedli, A. C.; Blancharddesce, M.; Perry, J. W.; Skindhoj, J. *Science* **1994**, *263* (5146), 511–514.
(13) Song, N. H.; Men, L. Q.; Gao, J. P.; Bai, Y. W.; Beaudin, A. M. R.; Yu, G. M.; Wang, Z. Y. *Chem. Mater.* **2004**, *16* (19), 3708–3713.
(14) Ashwell, G. J.; Hargreaves, R. C.; Baldwin, C. E.; Bahra, G. S.; Brown, C. R. *Nature* **1992**, *357* (6377), 393–395.
(15) Lupo, D.; Ringsdorf, H.; Schuster, A.; Seitz, M. *J. Am. Chem. Soc.* **1994**, *116* (23), 10498–10506.
(16) van der Boom, M. E.; Marks, T. J. *Polymers for Microelectronics and Nanoelectronics*; Oxford University Press: Oxford, U.K., 2004; Vol. 874, pp 30−43.
(17) Zhao, Y. G.; Chang, S.; Wu, A.; Lu, H. L.; Ho, S. T.; van der Boom, M. E.; Marks, T. J. *Opt. Eng.* **2003**, *42* (2), 298–299.
(18) Facchetti, A.; Abbotto, A.; Beverina, L.; van der Boom, M. E.; Dutta, P.; Evmenenko, G.; Pagani, G. A.; Marks, T. J. *Chem. Mater.* **2003**, *15* (5), 1064–1072.
(19) Zhu, P. W.; van der Boom, M. E.; Kang, H.; Evmenenko, G.; Dutta, P.; Marks, T. J. *Chem. Mater.* **2002**, *14* (12), 4982–4989.
(20) Liu, Z.; Ma, J.; Sun, D.; Xu, G.; Ho, S.; Zhu, P.; Kang, H.; Facchetti, A.; Marks, T. *Opt. Precis. Eng.* **2005**, *13* (5), 554–560.
(21) Zhifi, L.; Ho, S.; Chang, S.; Marks, T. *Technical Digest. Summaries of Papers Presented at the Conference on Lasers and Electro-Optics. Conference Edition (IEEE Cat. No. 02CH37337)*; Optical Society of America: Washington, D.C., 2002; Vol. 19, pp 6–197.
(22) Wasserman, S. R.; Tao, Y. T.; Whitesides, G. M. *Langmuir* **1989**, *5* (4), 1074–1087.
(23) Maoz, R.; Netzer, L.; Gun, J.; Sagiv, J. *J. Chim. Phys. Phys.-Chim. Biol.* **1988**, *85* (11–12), 1059–1065.
(24) Ulman, A. *Chem. Rev.* **1996**, *96* (4), 1533–1554.
(25) Guang, C.; Hong, H. G.; Mallouk, T. E. *Acc. Chem. Res.* **1992**, *25* (9), 420–427.
(26) Kepley, L. J.; Sackett, D. D.; Bell, C. M.; Mallouk, T. E. *Thin Solid Films* **1992**, *208* (1), 132–136.
(27) Lee, H.; Kepley, L. J.; Hong, H. G.; Akhter, S.; Mallouk, T. E. *J. Phys. Chem.* **1988**, *92* (9), 2597–2601.
(28) Dalton, L.; Robinson, B.; Nielsen, R.; Jen, A.; Steier, W. *Proc. SPIE−Int. Soc. Opt. Eng.* **2002**, *4798*, 1–10.
(29) Robinson, B. H.; Dalton, L. R.; Harper, A. W.; Ren, A.; Wang, F.; Zhang, C.; Todorova, G.; Lee, M.; Aniszfeld, R.; Garner, S.; Chen, A.; Steier, W. H.; Houbrecht, S.; Persoons, A.; Ledoux, I.; Zyss, J.; Jen, A. K. Y. *Chem. Phys.* **1999**, *245* (1–3), 35–50.

Scheme 1. Synthesis of the $+\beta$ Chromophore 1 and the $-\beta$ Chromophore 2

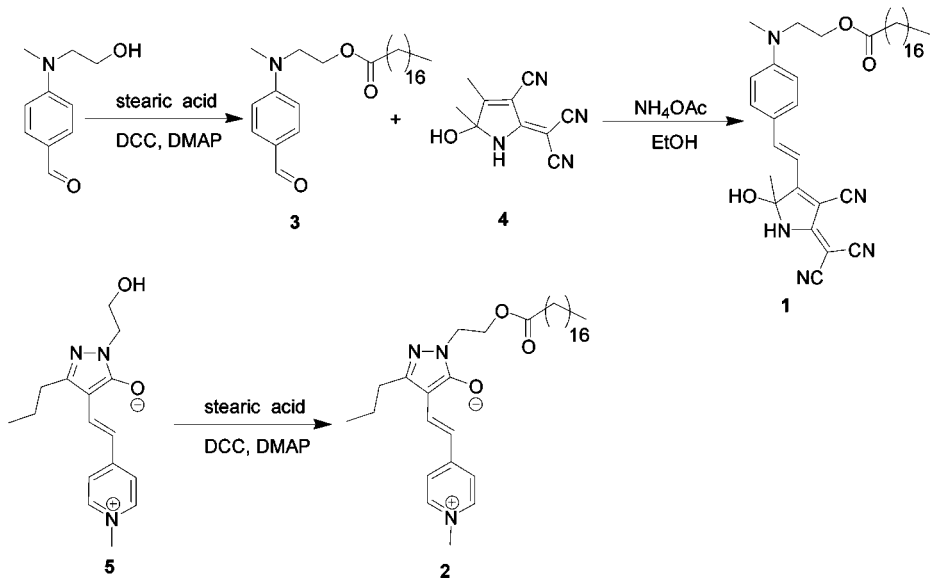

Experimental Section

Molecular Design. The $+\beta$ chromophore is conjugated at the electron donating group through an ester bridge to an 18-carbon chain. The $-\beta$ chromophore is similarly conjugated at the electron accepting group. The hydrophobic carbon chains are positioned on the $+\beta$ and $-\beta$ chromophores such that the dipole moments are antiparallel and the molecular hyperpolarizabilities are parallel when mixtures of the molecules are assembled at the air–water interface (Figure 1).

Synthesis of the Neutral Ground State ($+\beta$) and Zwitterionic ($-\beta$) Chromophores. The $+\beta$ chromophore **1** and the $-\beta$ chromophore **2** were synthesized as in Scheme 1. Both chromophores were stored dry at -20 °C for periods up to 6 months after synthesis.

Stearic Acid 2-[(4-Formyl-phenyl)-methyl-amino]-ethyl Ester (3). A mixture of 1.5 g (8.4 mmol) of 4-[(2-hydroxy-ethyl)-methyl-amino]-benzaldehyde and 2.7 g (9.5 mmol) of stearic acid was dissolved in 20 mL of dry dichloromethane. To the solution was added 2.1 g (10.2 mmol) of DCC and 0.16 g (1.3 mmol) of DMAP. After stirring overnight at room temperature, the mixture was added to 50 mL of diethyl ether. The insoluble solid was filtered off. The solvent of the filtrate was evaporated under reduced pressure. The remaining solid was dissolved in a minimum amount of dichloromethane. Methanol was added to the solution to precipitate 3.4 g of the product (91% yield). ^{1}H NMR (acetone-d_6): 0.89 (3H, t, $J = 6.7$ Hz), 1.20–1.40 (28 H, m), 1.52 (2H, quintet, $J = 7.2$ Hz), 2.24 (2H, t, $J = 7.4$ Hz), 3.14 (3H, s), 3.81 (2H, t, $J = 5.7$ Hz), 4.32 (2H, t, $J = 5.7$ Hz), 6.90 (2 H, d, $J = 9.0$ Hz), 7.73 (2H, d, $J = 9.0$ Hz), 9.74 (1H, s).

Chromophore **1.** To a mixture of 0.446 g (1 mmol) of **3** and 0.4 g (2 mmol) of **4** was added 2 mL of THF. After stirring, 8 mL of ethanol and 77.1 mg (1 mmol) of ammonium acetate were added to the mixture. After being stirred overnight, the reaction mixture was added to 100 mL of water. The crude product was extracted with ethyl acetate and purified using column chromatography with silica gel as the stationary phase and 1:9 ethyl acetate:dichloromethane as the mobile phase to give 0.28 g of **1** (45% yield). ^{1}H NMR (acetone-d_6): 0.89 (3H, t, $J = 6.7$ Hz), 1.20–1.40 (28 H, m), 1.53 (2H, quintet, $J = 7.3$ Hz), 1.88 (3H, s), 2.25 (2H, t, $J = 7.4$ Hz), 2.80 (1H, s), 3.17 (3H, s), 3.83 (2H, t, $J = 5.6$ Hz), 4.34 (2H, t, $J = 5.6$ Hz), 6.93 (2H, d, $J = 9.1$ Hz), 7.01 (2H, d, 16.0 Hz), 7.71(2H, d, $J = 9.0$ Hz), 7.97 (2H, d, 8.0 Hz). HRMS (ESP) *m/e*: 628.4148 (M + H).

Chromophore **2.** To a mixture of 355 mg (1.25 mmol) of stearic acid and 309 mg (1.5 mmol) of DCC was added 5 mL of dry dichloromethane. After stirring for 15 min, we added 26 mg (0.15 mmol) of DMAP to the mixture. After the mixture was stirred for another 10 min, 300 mg (1.04 mmol) of **5** was added and the mixture was stirred overnight at room temperature. After filtering off the insoluble solid, the solvent of the filtrate was evaporated under reduced pressure. The remaining solid was purified on silica gel column with 15% methanol in dichloromethane as the eluant to yield 500 mg of pure product (72%). ^{1}H NMR (MeOD): 0.92 (3H, t, $J = 6.7$ Hz), 1.00 (3H, t, $J = 7.9$ Hz), 1.20–1.40 (28 H, m), 1.56 (2H, quintet, $J = 7.1$ Hz), 1.68 (2H, hexalet, 7.5 Hz), 2.31 (2H, t, $J = 7.4$ Hz), 2.60 (2H, t, 7.5 Hz), 4.0 (1H, s), 4.03 (2H, t, $J = 5.7$ Hz), 4.33 (2H, t, $J = 5.7$ Hz), 6.95 (2H, d, $J = 15.4$ Hz), 7.52 (2H, d, 6.7 Hz), 7.76 (2H, d, 15.4 Hz), 8.04 (2H, d, 6.7 Hz). HRMS (ESP) *m/e*: 554.4243 (M + H).

Langmuir Monolayers and Langmuir–Blodgett Deposition. Chromophores were dissolved in chloroform at 0.25–1 mg/mL and used within 24 h. Chromophore solutions were deposited at the air/buffer interface of 15 mM sodium bicarbonate buffer (pH 8.0–8.5) in a home-built Langmuir trough similar to those described previously.[30] All Langmuir monolayer measurements and film transfers were conducted under an inert Argon atmosphere to prevent oxidation of the chromophores. Monolayers containing $+\beta$ and $-\beta$ chromophores in molar ratios of 0:4, 1:7, 1:3, 3:5, 1:1, 3:1, and 4:0 were compressed and expanded over three cycles to generate pressure–area isotherms. Langmuir–Blodgett monolayers were deposited on either glass coverslips for fluorescence microscopy or on gold-coated silicon for atomic force microscopy. All films had transfer ratios of approximately 1, meaning that the monolayer area lost on the trough was approximately equal to the area of the film deposited on the substrate. Glass slides were cleaned by boiling in 7× Cleaning Solution (ICN Biomedicals, Aurora OH) diluted in 18 MΩ-cm water (1:4), rinsed with copious amounts of 18 MΩ-cm water, dried under an N_2 stream, then plasma cleaned before use. For deposition of Langmuir–Blodgett multilayers, a KSV 5000 trough (KSV, Trumbull CT) with alternate-multilayer capabilities was used.

Fluorescence Microscopy. Both the $+\beta$ and $-\beta$ chromophores are weakly fluorescent, and deposited monolayers were imaged on

(30) Halter, M.; Nogata, Y.; Dannenberger, O.; Sasaki, T.; Vogel, V. *Langmuir* **2004**, *20* (6), 2416–2423.

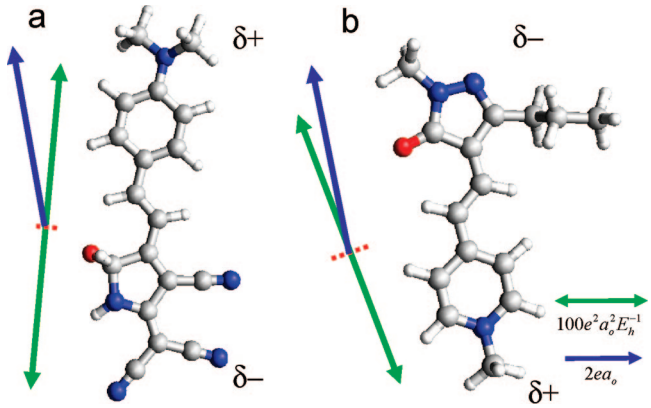

Figure 2. Representations of the calculated resonance hyperpolarizabilities of the (a) $+\beta$ and (b) $-\beta$ chromophores (λ_{max} = 543 and 530 nm, respectively, with an SHG wavelength of 532 nm in these measurements). Alkyl chains (not shown) are near the top of each chromophore. The nonlinear polarizabilities are dominated by interactions along the long molecular axes of both molecules and are of identical sign. The single-sided arrows in blue indicate the transition moments of the dominant, resonant excited state, and the other lines indicate the principal elements of the two-photon absorption tensor to the same state, with solid green and dashed red indicating positive and negative sign, respectively. The scale bars are in atomic units, with e indicating elementary charge, a_o the Bohr radius, and E_h the Hartree energy.

a TE2000 inverted fluorescence microscope (Nikon, Melville, NY) with a 100x× oil immersion lens (1.4 N.A.) using a mercury arc lamp source, a standard Texas-Red fluorescence filter cube set, and a CoolSNAP HQ CCD camera (Photometrics, Tucson, AZ).

Atomic Force Microscopy (AFM). AFM images were acquired using an MFP-3D atomic force microscope (Asylum Research, Santa Barbara, CA) in intermittent contact mode, using BS-Tap300 cantilevers (Budget Sensors, Sofia, Bulgaria) with spring constants of ∼40 N/m and resonance frequencies of ∼300 kHz.

Quantum Chemical Calculations. The resonant hyperpolarizabilities of the $+\beta$ and $-\beta$ chromophores were calculated using the AM1 semiempirical method in Gaussian 98. Under conditions of resonance enhancement at or near the second harmonic frequency, the resonant $\beta^{(2)}$ tensor rigorously reduces to the direct product of the one-photon transition moment and the tensor for two photon absorption.[31,32]

$$\beta^{(2)}(-2\omega;\omega,\omega) = -S(2\omega)\mu_{0n}^{(0)} \otimes \alpha_{n0}^{(1)} \quad (1)$$

The line shape function $S(2\omega)$ (e.g., Lorentzian) is purely imaginary on resonance at 2ω, with the real part inverting in sign across the transition. The two photon absorption tensors were determined by a sum-over states calculation including ∼100 excited states to achieve convergence. The results of the calculations can be represented using single-sided and double-sided arrows for the transition moment and the principal moments of the two-photon absorption tensor, respectively (Figure 2).[33,34]

Nonlinear Optical Ellipsometry (NOE). NLO ellipsometry measurements were performed to determine the relative signs and magnitudes of the nonzero surface $\chi^{(2)}$ tensor elements. The instrumentation and algorithms for data analysis have been described in detail previously[35,36] and will be only briefly summarized. All measurements were acquired using the 1064 fundamental wavelength of a Q-switched Nd:YAG laser (New Wave, ∼5–7 ns and ∼13 mJ pulses, unfocused) with measurements acquired in transmission at an angle of 45°. The polarization state of the incident 1064 nm beam was prepared to be either linearly polarized with the polarization axis oriented at 45° with respect to the plane of reflectance or circularly polarized by appropriate rotation angles of half- and quarter-wave plates. The frequency doubled beam was spectrally isolated by a combination of Schott glass filters and interference filters. The complex polarization state of the second harmonic generation (SHG) beam was obtained from fits of the detected horizontally and vertically polarized intensities, I, as functions of the rotation angle of a quarter wave plate. Both sets of the resulting raw data were fit to the following general equation.

$$I_{det}^{2\omega} \propto K\sin(2\alpha_Q^{2\omega}) + L\sin(4\alpha_Q^{2\omega}) + M\cos(4\alpha_Q^{2\omega}) + N \quad (2)$$

The complete polarization state of frequency doubled beam can be calculated from the parameters K, L, M, and N obtained from the fits. For a polarizer set initially to pass p-polarized light, the complete polarization state, ρ, of the SHG beam is given by the following equation.

$$\rho_{p\text{-polarized}} \equiv \frac{e_p^{2\omega}}{e_s^{2\omega}} = \frac{M+N}{2L-iK} \quad (3)$$

If the detection geometry is changed such that the final fixed polarizer passes s-polarized light, the expression for ρ changes to the following equation.

$$\rho_{s\text{-polarized}} = \frac{-2L-iK}{M+N} \quad (4)$$

Two independent measurements of ρ were obtained for each quarter-wave rotation experiment using both eqs 3 and 4 by including a separate detector for each polarization component at the polarizing beam-splitter.

The experimentally measured complex values of ρ can, in turn, be related directly back to a generalized model-independent 2 × 2 × 2 Jones tensor describing surface NLO properties.[36] In the case of SHG for an achiral uniaxial film such as that described in this work, only three nonzero independent elements within the Jones tensor remain (χ_{PPP}, χ_{Pss}, and χ_{ssP}).

$$\rho = \frac{\chi_{ppp}(e_p^{\omega})^2 + \chi_{pss}(e_s^{\omega})^2}{2\chi_{ssp}e_s^{\omega}e_p^{\omega}} \quad (5)$$

The elements of the Jones tensors are complex functions of the angle of incidence, the optical constants of the interfacial layer at all relevant wavelengths, the refractive indices and thickness of the SHG-active interfacial layer, and the nonlinear optical properties of the interface itself.[37,38] Using an appropriate thin film model for the interfacial optics allows inversion of the Jones $\chi^{(2)}$ tensor elements into Cartesian $\chi^{(2)}$ tensor elements, which can in turn be used to interpret molecular structure and surface orientation.

(31) Moad, A. J.; Simpson, G. J. *J. Phys. Chem. B* **2004**, *108* (11), 3548–3562.
(32) Moad, A. J.; Simpson, G. J. *J. Phys. Chem. A* **2005**, *109* (7), 1316–1323.
(33) Perry, J. M.; Moad, A. J.; Begue, N. J.; Wampler, R. D.; Simpson, G. J. *J. Phys. Chem. B* **2005**, *109* (42), 20009–20026.
(34) Wampler, R. D.; Zhou, M.; Thompson, D. H.; Simpson, G. J. *J. Am. Chem. Soc.* **2006**, *128* (34), 10994–10995.
(35) Plocinik, R. M.; Simpson, G. J. *Anal. Chim. Acta* **2003**, *496* (1–2), 133–142.
(36) Plocinik, R. M.; Everly, R. M.; Moad, A. J.; Simpson, G. J. *Phys. Rev. B* **2005**, *72* (12).
(37) Heinz, T. F. Second Order Nonlinear Optical Effects at Surfaces and Interfaces. In *Nonlinear Surface Electromagnetic Phenomena*; North-Holland: New York, 1991; pp 354–416.
(38) Simpson, G. J.; Dailey, C. A.; Plocinik, R. M.; Moad, A. J.; Polizzi, M. A.; Everly, R. M. *Anal. Chem.* **2005**, *77* (1), 215–224.

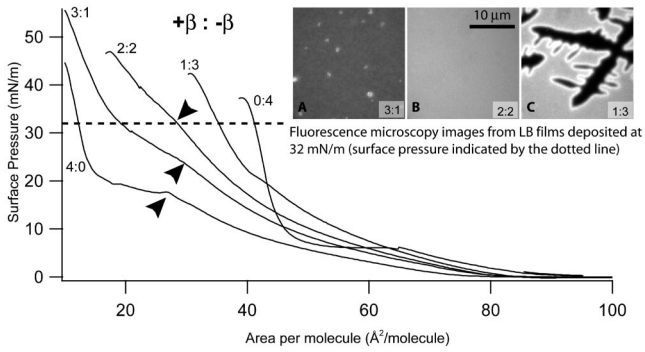

Figure 3. Surface pressure versus area isotherms are shown for mixtures of the $+\beta$ and $-\beta$ chromophores. Isotherms from monolayers rich in the $+\beta$ chromophore exhibit a kink at molecular areas ranging from 29 to 34 Å^2/molecule (kink locations indicated by arrowheads). At the kink, the isotherm slope decreases upon compression, suggesting a collapse transition. Fluorescence images are shown from Langmuir–Blodgett films deposited at 32 mN/m (indicated by the dashed line) from $+\beta$:$-\beta$ mixtures with ratios of (A) 3:1, (B) 1:1, and (C) 1:3. Film (A) was deposited above the kink, (B) was deposited before the kink, and the 1:3 composition (C) did not exhibit a kink in the isotherm.

Measurements of polarization states, ρ, for circular and linear incident light allow eq 1 to be inverted to yield a set of complex-valued elements of the Jones and Cartesian $\chi^{(2)}$ tensors

$$\frac{\chi_{pss}}{\chi_{ssp}} = -[\rho_{-45} + i\rho_R] = \frac{s_{ZYY}\chi_{ZXX}}{s_{YYZ}\chi_{XXZ}} \tag{6a}$$

$$\frac{\chi_{ppp}}{\chi_{ssp}} = -[\rho_{-45} - i\rho_R] = \frac{\mp s_{XXZ}}{s_{YYZ}} + \frac{s_{ZXX}\chi_{ZXX}}{s_{YYZ}\chi_{XXZ}} + \frac{s_{ZZZ}\chi_{ZZZ}}{s_{YYZ}\chi_{XXZ}} \tag{6b}$$

The subscripts on ρ in eqs 6a and 6b indicate the polarization state of the incident beam in the a given measurement of ρ, with R indicating right circular polarization and $-45°$ indicating linearly polarized light with the axis of polarization oriented $-45°$. Using eq 6a and 6b, the Jones and Cartesian tensor elements can be directly obtained with full retention of relative sign and phase information from differences of the measured values for ρ once the s coefficients are determined using an appropriate thin film model.

Results

Mixing $+\beta$ and $-\beta$ Chromophores Increases Monolayer Stability. The $+\beta$ and $-\beta$ amphiphilic chromophores in Figure 1 were designed to produce favorable electrostatic interactions when mixed in Langmuir monolayers, due to the antiparallel alignment of their molecular dipole moments. As intended, monolayers of mixed $+\beta$ and $-\beta$ chromophores were more stable than monolayers of either pure chromophore. Specifically, we used Langmuir trough isotherms, fluorescence microscopy, AFM, and creep tests to show that monolayers containing mixtures of the chromophores produce homogeneous layers able to withstand higher surface pressures than monolayers containing either pure chromophore. We will discuss the results of each technique in turn.

Pressure–area isotherms of chromophore monolayers appear in Figure 3. The isotherms provide two lines of evidence that monolayers rich in the $+\beta$ chromophore are unstable and collapse under lateral pressure. First, these monolayers

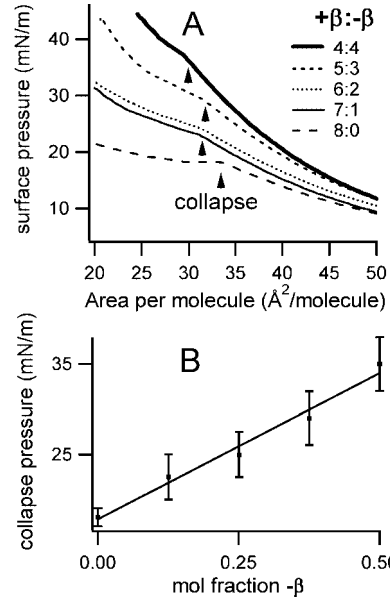

Figure 4. (A) Surface pressure vs area isotherms from mixed $+\beta$:$-\beta$ films. As the fraction of $-\beta$ chromophore in the $+\beta$ monolayer is decreased from 8:0 (100%) to 4:4 (50%), the surface pressure at which the kink appears in the isotherm increases. Kink locations are indicated by arrows. (B) The surface pressure at which the kink occurs was averaged from three separate isotherm measurements and plotted for each mole fraction of $-\beta$ chromophore. Error bars represent the entire range of largest and smallest values for the observed kink in the isotherm.

compress to molecular areas approaching zero. Since the limiting molecular area for a close-packed monolayer of saturated fatty acids is ~20 Å^2/molecule, the $+\beta$ monolayers must have collapsed at molecular areas <20 Å^2/molecule. The collapse process is reversible because isotherms are reversible over several compression and expansion cycles (data not shown). Second, isotherms of monolayers rich in the $+\beta$ chromophore exhibit a sudden decrease of slope between ~29 and 34 Å^2/molecule (marked by arrowheads in Figure 3). This kink in the isotherm is investigated more closely in Figure 4.

Increasing the fraction of $-\beta$ chromophore in the monolayer of $+\beta$ chromophore linearly increases the average surface pressure at which the kink occurs (Figure 4). Increasing collapse pressure indicates an increasing resistance to buckling. In other words, by mixing the two chromophores, monolayers are able to withstand higher surface pressures before collapse. Because the area under the pressure–area isotherm up to the point of collapse is proportional to the energy required to buckle the monolayer, the data in Figure 4 illustrate a favorable self-assembly of the mixed chromophore system.

Fluorescence microscopy and AFM were employed to verify whether monolayers containing high $+\beta$ chromophore fractions indeed collapsed. Monolayers of 3:1 of $+\beta$:$-\beta$ chromophore deposited at 32mN/m on substrates contain bright fluorescent punctate features on a darker background (Figure 3a). For this composition, 32mN/m is above the kink in the isotherm. Atomic force microscopy shows that the bright features are domains of two step heights (Figure 5a), consistent with monolayer collapse. The composition of these aggregates is addressed below in the discussion section.

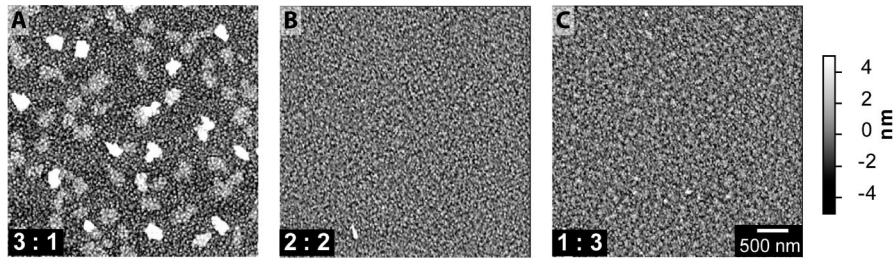

Figure 5. AFM images from Langmuir–Blodgett films deposited from mixtures of $+\beta$:$-\beta$ chromophore monolayers onto gold coated Si wafers at 32 mN/m. (A) The topographical features in the 3:1 mixture indicate collapse of the monolayer. (B) and (C) The smooth topography of the 2:2 and 1:3 mixtures indicate the absence of monolayer collapse. The surface roughness of the monolayers in (B) and (C) corresponds to the surface roughness of bare gold films.

In contrast, for equimolar concentrations of $+\beta$ and $-\beta$ chromophores, monolayers resist collapse to surface pressures above 32 mN/m. Evidence to support this claim is that the kink in the isotherm occurs above 32 mN/m (Figure 3), and that the deposited monolayer is uniform, as observed by both fluorescence microscopy (Figure 3b), and by AFM (Figure 5b). In summary, for equimolar $+\beta$ and $-\beta$ mixtures, the two chromophores appear highly miscible at surface pressures $\leq$32 mN/m.

Monolayers containing high (rather than low) concentrations of $-\beta$ chromophore resist collapse, but face a different problem. Fluorescence microscopy shows dark domains in monolayers deposited at 32 mN/m monolayers containing 1:3 of $+\beta$:$-\beta$ chromophore (Figure 3c). Phase separation has occurred. The dark domains are most likely rich in the $-\beta$ chromophore because the $+\beta$ chromophore is more strongly fluorescent. Chromophores in the dark regions may be aligned in weakly fluorescent J-aggregates, which are known to form in Langmuir monolayers containing zwitterionic dyes.[39,40] Modifying the $+\beta$ chromophore by adding a second alkyl chain at the same position via a tertiary amine does not eliminate the formation of domains (data not shown). Domains must be within the plane of the monolayer because AFM shows that deposited monolayers containing 1:3 of $+\beta$:$-\beta$ chromophore are topographically smooth (Figure 5c).

Monolayers of pure $-\beta$ chromophore are particularly unstable. In this case, monolayer stability was assessed by compressive creep tests[41] in which the monolayer pressure was held constant and the monolayer area was monitored with time. As shown in Figure 6, monolayers spread from pure $-\beta$ chromophore solutions exhibit substantial creep compared with monolayers spread from 1:1 and 1:3 ($+\beta$:$-\beta$) mixed solutions. Because the chromophores absorb light in the visible spectrum, the location of the chromophores in the trough can be evaluated by eye. Throughout the creep experiment, the chromophores remained confined between the trough barriers and no color was observed in the subphase or outside the barriers. This implies that chromophores do not irreversibly leave the interface while the monolayer is under compression, which is consistent with our earlier observations of reversible isotherms.

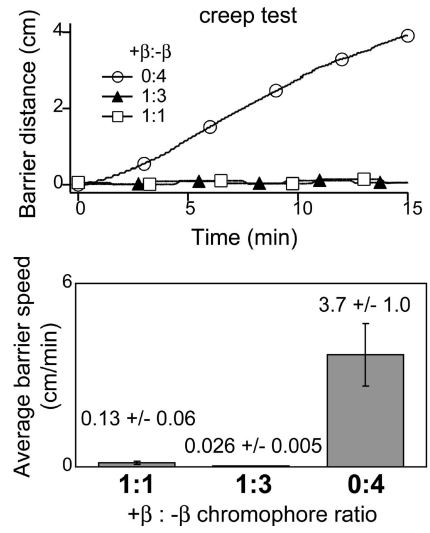

Figure 6. Compressive creep tests were performed according to the method described by Biddle et al.,[41] where the surface pressure was held constant at 32 mN/m. (A) The barrier's lateral movement is plotted against time for each of the chromophore mixtures. (B) The average velocity of the barrier for a 15 min interval is graphed for the each of the chromophore mixtures.

Film Reorganization. The results above imply that films of equimolar $+\beta$:$-\beta$ chromophores are uniformly mixed and stable. Here, we investigate the long-term stability of chromophore films after deposition on a solid surface. Monolayers of equimolar $+\beta$:$-\beta$ chromophore concentration are uniform immediately after Langmuir–Blodgett deposition (Figures 3b and 5b), but exhibit micron-scale arrow-shaped aggregates after 9 h at 65 °C (Figure 7). By fluorescence microscopy, the contrast of the domains reverses through time. Initially the aggregates are bright (Figure 7a), but brief (<5 s) exposure to the fluorescence–excitation source inverts the contrast as in Figure 7b. Continued illumination (1–2 min) photobleaches the background but not the aggregates, and the contrast is inverted once more as in Figure 7c.

Atomic force microscopy reveals that most aggregates protrude 2 nm above the background monolayer surface (Figure 7d). Phase AFM finds significant contrast differences between the aggregates and the background, indicating that the two regions have distinct surface properties. A few (<10%) of the aggregates form multilayered structures at discrete heights of 2 nm, 6 and 8 nm above the background. Topographical and phase images are shown in images f and g in Figure 7.

(39) Mizrahi, V.; Stegeman, G. I.; Knoll, W. *Phys. Rev. A* **1989**, *39* (7), 3555–3562.
(40) Nakahara, H.; Fukuda, K.; Mobius, D.; Kuhn, H. *J. Phys. Chem.* **1986**, *90* (23), 6144–6148.
(41) Biddle, M. B.; Rickert, S. E.; Lando, J. B. *Thin Solid Films* **1985**, *134* (1–3), 121–134.

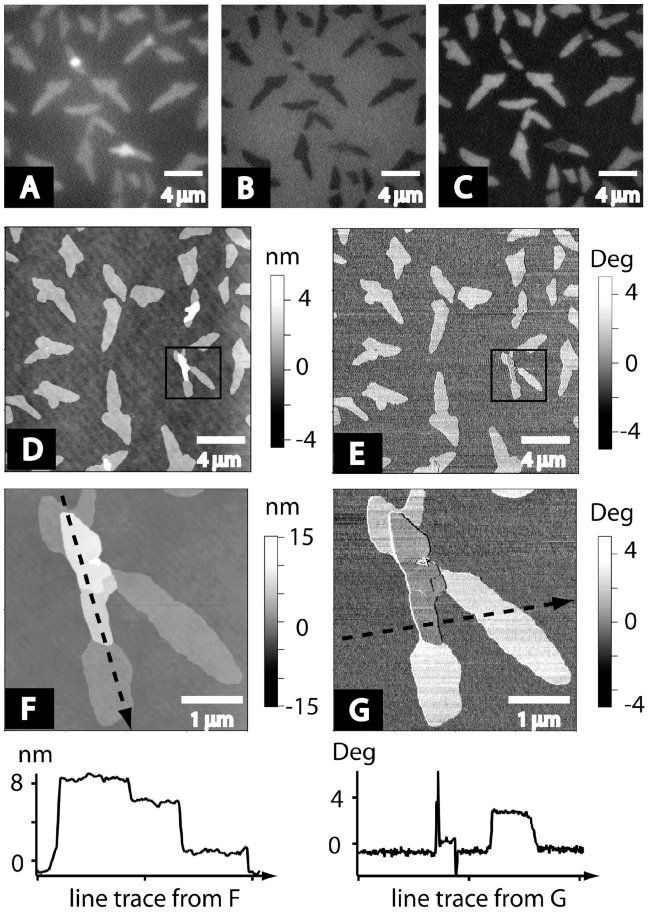

Figure 7. (A−C) Monolayer film of a 1:1 ($+\beta$:$-\beta$) chromophores after LB deposition and storage at 65 °C for 9 h. Aggregates have formed. Fluorescence images were acquired after exposure of the substrate to illumination, either after no time had elapsed (A), after several seconds had elapsed (B), or after several minutes had elapsed (C). (D, E) Topographical and phase AFM images, respectively, of the 1:1 ($+\beta$:$-\beta$) monolayer film exhibiting aggregates. (F, G) High-resolution AFM images from the corresponding boxed regions in (D, E) of a multilayered aggregate. The line trace below (F) follows the dashed line in (F) and shows well-defined feature heights at 2, 6, and 8 nm above the background. The line trace below (G) follows the dashed line in (G) and shows phase differences between the different regions of the aggregate, indicating differences in surface chemistry.

Nucleation and growth of domains is shown in Figure 8 for a monolayer deposited from a 1:1 ($+\beta$:$-\beta$) mixture. The LB film was held at room temperature and imaged over an 88 h period. The freshly deposited monolayer exhibits uniform fluorescence (Figure 8a). Aggregates nucleate (Figure 8b) and increase in size over time. At intermediate times, halos of brighter fluorescence surround the aggregates, presumably the result of depletion of the either the $+\beta$ or the $-\beta$ chromophore as the aggregate grows (images c and d in Figure 8). Eventually, the background fluorescence becomes uniform (Figure 8e). Aggregates are stable for several months.

High temperature rapidly escalates aggregate nucleation and growth. After only 9 h at 23 °C, the nucleation and growth of aggregates is comparable to those of aggregates on a film maintained for 60 h at 4 °C (Figure 9). Similarly, after only 9 h at 65 °C, well-developed aggregates are similar to those on a film maintained for 60 h at 23 °C (data not shown). Moreover, a sample maintained at the low temperature of −20 °C develops only small aggregates after the long time of 160 h.

The rearrangement of films in air is surprising when compared with previous data from the literature. Fatty acid monolayers and multilayers are typically stable in air and rearrange only under aqueous conditions.[42,43] In our system, mixing the molecules at the air/buffer interface enhances the monolayer stability, but, surprisingly, under dry conditions the molecules within the film aggregate into distinct structures. The molecules are apparently prevented from forming aggregates at the air/buffer interface, possibly because of the high interfacial energy experienced by these amphiphilic chromophores at the surface of the Langmuir trough.

We also attempted to construct multiple alternate layer films with an interleaved poly(tert)-butyl methacrylate layer (data not shown). Previous investigations using layer-by-layer deposition of LB films interleaved with poly(tert)-butyl methacrylate have reported long-term stability (several months to years) with films containing up to 160 layers.[44–48] In our system, multilayer films interleaved with poly(tert)-butyl methacrylate had reduced NLO activity compared to monolayer films, probably because molecular rearrangements occurred while the film sequentially passed through the air/buffer interface.

LB Film Structure. The high NLO activity of our LB films allowed efficient detection of second harmonic generation (SHG) from a single monolayer without requiring focusing of the incident beam. Interestingly, the relative intensities of the 1:1 mixed film was ∼5 fold smaller than the pure $+\beta$ film. An interpretation consistent with this result is that the nonlinear optical response of the film is dominated by the $+\beta$ chromophore. In this case, a 50% reduction in surface density upon dilution with the $-\beta$ chromophore would yield a ∼4-fold reduction in the detected SHG intensity. This interpretation is supported by hyper-Rayleigh-scattering measurements for different wavelengths (880 and 440 nm) that suggest that the $-\beta$ chromophore exhibits significantly weaker NLO activity.[49] On the other hand, the calculated NLO activities of the $+\beta$ and $-\beta$ chromophores are comparable, so the microscopic origin of the apparent dominance of the $+\beta$ chromophore in both the pure and mixed films is not immediately clear. Differences between the calculated and measured values may potentially be attributed to strong intermolecular interactions driving largely antiparallel packing of the $-\beta$ chromophore.

(42) Takamoto, D. Y.; Ter-Ovanesyan, E.; Schwartz, D. K.; Viswanathan, R.; Chiruvolu, S.; Zasadzinski, J. A. *Acta Phys. Pol., A* **1998**, *93* (2), 373–382.
(43) Takamoto, D. Y.; Ter-Ovanesyan, E.; Zasadzinski, J. A. *Biophys. J.* **1998**, *74* (2), A186–A186.
(44) Ashwell, G. J.; Whittam, A. J. *Mol. Cryst. Liq. Cryst.* **1999**, *337*, 1–6.
(45) Ashwell, G. J. *J. Mater. Chem.* **1999**, *9* (9), 1991–2003.
(46) Ashwell, G. J.; Zhou, D. J.; Skjonnemand, K.; Ranjan, R. *Aust. J. Chem.* **2001**, *54* (1), 19–25.
(47) Cha, J.; See, Y. K.; Lee, J.; Chang, T. *Synth. Met.* **2001**, *117* (1–3), 149–152.
(48) Cha, J.; Shin, H. S.; See, Y. K.; Lee, J.; Chang, T.; Kim, S. B. *Synth. Met.* **2001**, *117* (1–3), 169–171.
(49) Liao, Y.; Bhattacharjee, S.; Firestone, K. A.; Eichinger, B. E.; Paranji, R.; Anderson, C. A.; Robinson, B. H.; Reid, P. J.; Dalton, L. R. *J. Am. Chem. Soc.* **2006**, *128* (21), 6847–6853.

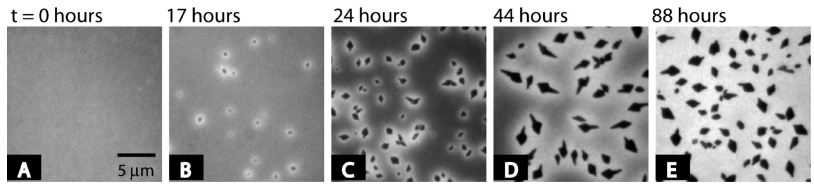

Figure 8. Fluorescence microscopy images demonstrating the nucleation and growth of aggregates within a deposited monolayer of a 1:1 ratio of $+\beta$:$-\beta$ chromophores stored in open air at room temperature. t= (A) 0, (B) 17, (C) 24, (D) 44, and (E) 88 h. Images were contrast-enhanced on a linear scale to illustrate fluorescence distribution during aggregate growth.

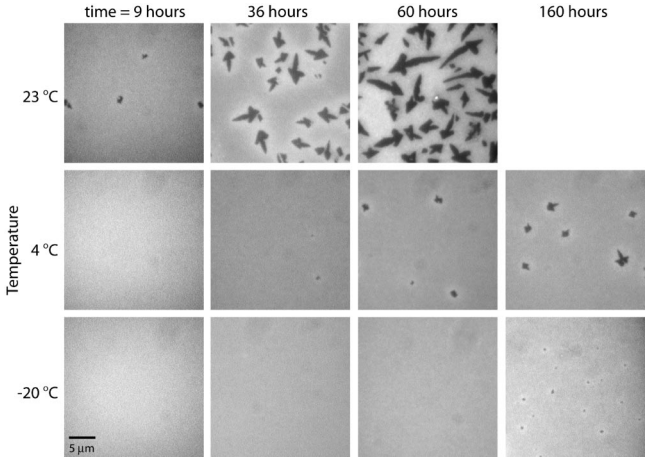

Figure 9. Fluorescence micrographs showing aggregate formation within deposited monolayers of a 1:1 ratio of $+\beta$:$-\beta$ chromophores stored at temperatures ranging from 23 to –20 °C over a period of ≤160 h. Decreased temperature substantially slows aggregate growth.

Polarization dependent nonlinear optical ellipsometry (NOE) was used to characterize the structure of the LB films (Figure 10). By analogy with linear ellipsometry, NOE polarization measurements yield the complete complex-valued ratios of the Jones $\chi^{(2)}$ tensor elements, from which polarization-dependent observables in a given measurement's configuration can be predicted. Assessing the orientation of the chromophores is critical for determining the effectiveness of this mixed chromophore approach for fabricating NLO materials. Furthermore, the aggregate formation and structure in these films may be important for understanding aggregation in technologically relevant NLO materials because the $+\beta$ chromophore is similar in structure to chromophores used in commercially available NLO devices.

Measurements acquired from monolayers several days after LB deposition indicated significant imaginary components within ratios of the nonzero $\chi^{(2)}$ tensor elements. There are three possible explanations for complex components in the ratios, 1) resonance effects, 2) a breakdown of the "effective medium approximation", and 3) chromophore aggregation. Although we will discuss all three reasons, the third is the most likely. First, individual $\chi^{(2)}$ tensor elements are generally complex near resonance. However, this fact in itself does not explain complex-valued ratios. If the dominant resonance-enhancement arises with a single spectroscopically isolated transition, as is suggested by quantum chemical calculations, then the $\chi^{(2)}$ tensor elements should all be described by the same complex-valued line shape function and yield purely real ratios.

A second possible explanation for the observation of complex terms within $\chi^{(2)}$ tensor elements lies in a possible

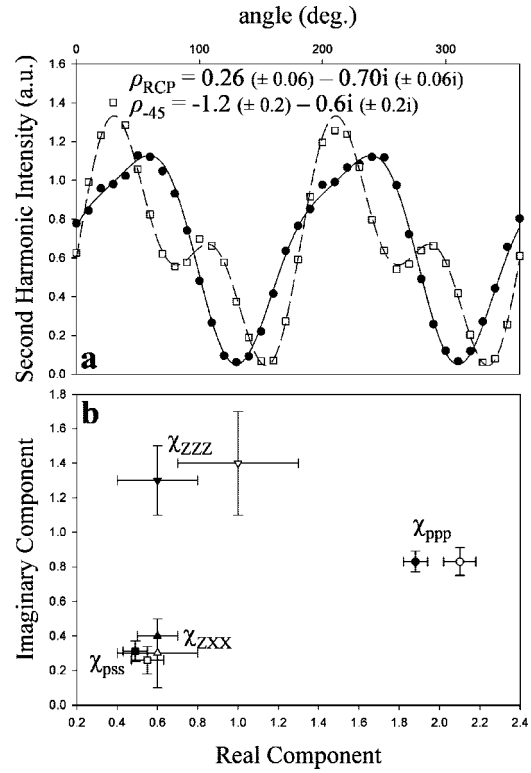

Figure 10. Overview of NOE polarization analysis for deposited LB monolayers. (a) Representative nonlinear optical ellipsometry measurements using a rotating quarter waveplate ellipsometry configuration in which the quarter wave plate rotation angle is indicated by the top axis for right circularly polarized light incident on a monolayer of a 1:1 ratio of $+\beta$:$-\beta$ chromophores in LB films (•) or linearly polarized light at –45° incident on a monolayer of pure $+\beta$ chromophore (□). (b) Resulting set of complex-valued Jones and Cartesian $\chi^{(2)}$ tensor elements (normalized to χ_{ssp} and χ_{XXZ}, respectively). Filled symbols (e.g., χ_{pss} (■), χ_{ppp} (•), χ_{ZXX} (▲), and χ_{ZZZ} (▼)) give values for pure $+\beta$ LB films, and open symbols give corresponding values for 1:1 $+\beta$:$-\beta$ LB films.

breakdown of the effective medium approximation used to generate Fresnel factors.[38] Near resonance, complex terms in the ultrathin film refractive index can result in complex components in corresponding Jones tensor elements. If the effective medium approximation does not properly account for complex components within the Fresnel factors, complex ratios of the Cartesian $\chi^{(2)}$ tensor elements can result solely from improper treatment of the interfacial optics. Indeed, in previous work using the same equipment, complex contributions in measured tensor elements were critical in originally validating the effective medium approximation for generating Fresnel factors.[38] In the present study, a $+\beta$ chromophore oriented with the alkyl chain away from the surface would yield a positive χ_{ZZZ}, which would result in a negative imaginary element in χ_{ZZZ}/χ_{ZZZ} because a factor of $(+i\kappa)$

appears in the denominator of the Fresnel factor for χ_{ZZZ} (where κ is the positive-signed imaginary component of the interface refractive index at the doubled frequency). The positively signed imaginary contribution observed in Figure 10 would require the opposite absolute molecular orientation for the $+\beta$ chromophore (i.e., with the alkyl chains oriented toward the substrate), which is unlikely for films prepared by LB deposition onto hydrophilic substrates. Therefore, we can discount the second explanation.

The third, and most likely, explanation for the measured phase difference is aggregation of chromophores in the films. The electronic states of two (or more) closely interacting neighboring chromophores can mix to form sum and difference states with unique resonance-enhancements and polarization-dependent linear and nonlinear optical properties.[32] Interference between the NLO responses of the monomers and the aggregates exhibiting exciton coupling can potentially result in complex-valued ratios of measured $\chi^{(2)}$ tensor elements. On the basis of these arguments, complex components within the molecular tensor indicate significant aggregation within the monolayer films, in good agreement with the fluorescence results presented earlier. In principle, it is possible to extract information on the structures and orientations of different exciton states from analysis of NOE measurements. In practice, the large number of unknown parameters (the orientation of each aggregate, the orientation of the monomers, the distributions in orientation for each, the fraction of molecules in monomer vs aggregate states, and the resonance frequencies associated with the sum and difference states in the aggregates) significantly complicates analysis of NOE measurements acquired at a single wavelength. Consequently, our analysis of the NOE data will be restricted to qualitative interpretations.

Quantum chemical calculations for the $+\beta$ and $-\beta$ chromophores suggest molecular tensors dominated by the long-axis β_{zzz} tensor element. In this limit, a broad distribution in orientation angles would be expected to produce a ratio of $\chi_{ZZZ}/\chi_{XXZ} \cong 3$, with values higher than 3 indicating preference toward tilt angles closer to the surface normal and values lower than 3 indicating preference toward orientations more parallel to the surface plane. Consequently, the data in Figure 10 are consistent with films exhibiting significant aggregation with chromophores preferentially adopting relatively high tilt angles away from the surface normal (i.e., greater than the magic angle of 39.2°).

Discussion

Film structures consistent with our fluorescence microscopy, AFM, and NOE results are shown in Figure 11. At the air/buffer interface, the $+\beta$ and $-\beta$ chromophores mix and form homogeneous ordered monolayers (Figure 11a). Upon Langmuir–Blodgett transfer to a hydrophilic support, nucleation of self-associated aggregates ($+\beta/+\beta$ and $-\beta/-\beta$) begins, followed by temperature-dependent growth (Figure 11b). In this proposed mechanism, the relatively large interfacial energy of the air/buffer interface constrains the molecules to the surface and favorable electrostatic interactions promote the miscibility of $+\beta$ chromophore with the $-\beta$ chromophore. When the films are transferred to a solid

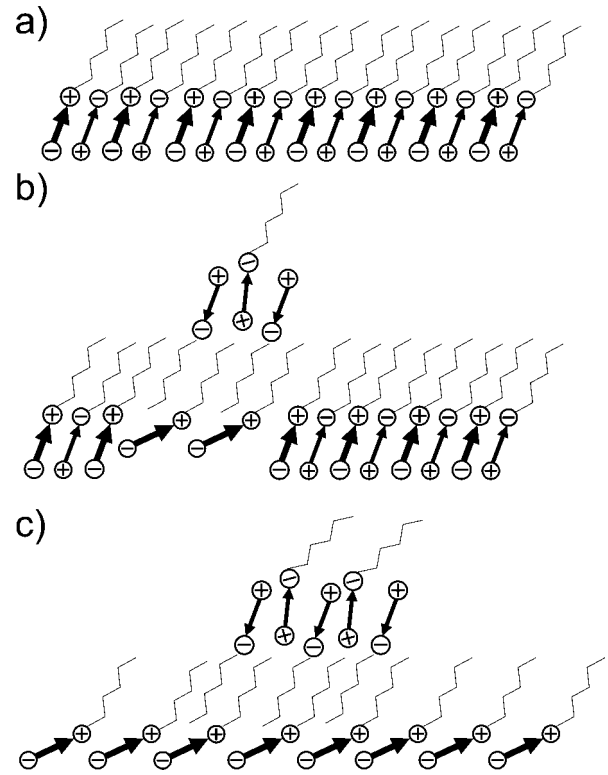

Figure 11. Proposed structures for a monolayer containing a 1:1 ratio of $+\beta$:$-\beta$ chromophores (A) at the air/buffer interface, (B) upon deposition to a substrate and after nucleation of aggregates, and (C) after equilibration with time and after growth of aggregates.

support, self-association of the constituent molecules dominates and aggregates form. Growth terminates after aggregates reach microns in size. Aggregates are primarily 2 nm above the background (Figure 11c). A rigorous confirmation of the film structures proposed in Figure 11 is challenging. Nevertheless, our proposed sequence of aggregation and growth accounts for all of our observations from each characterization technique. Below we will discuss the results that led to the construction of Figure 11.

The molecular packing densities of monolayers of mixed chromophore films at the air/buffer interface indicate the formation of close-packed, single monolayer films. The stability of the mixed films suggests the ordered structure in Figure 11a, where both the electrostatic interactions of the chromophores and van der Waals interactions of the hydrophobic chains are favorable. The structure appears to be maintained immediately after LB transfer of the films to a solid support because fluorescence microscopy images of the films are uniform and the topography measured by AFM is featureless.

The LB-transferred films form aggregates surrounded by depletion zones through a temperature-dependent nucleation and growth process. This is consistent with Figure 11b where the $-\beta$ chromophores nucleate into H-aggregates that extend above the film. We know that the aggregation process does not consume all of the surface material because fluorescence is emitted from both the aggregates and the background. The unusual photobleaching behavior of the aggregates (Figure 7) is also consistent with our model. The fast photobleaching material corresponds to the top layer of $-\beta$ chromophore and the slow photobleaching material corresponds to $+\beta$

chromophores protected from photooxidation by the aggregate. The uniform height of the aggregates (2 nm) indicates a thin, monomolecular film as in Figure 11c. Tapping mode AFM images seen in Figure 7 demonstrate a phase difference between the aggregates and the background that corresponds to their different surface chemistries.

Conclusion

Although the chromophores investigated here self-assemble into impressively stable monolayers at the air/buffer interface, efficient retention of the large molecular hyperpolarizabilities into multilayer films was not observed. A significant challenge for producing bulk NLO materials is controlling the packing and aggregation of chromophores. In the present system, the addition of the weak $-\beta$ chromophore resulted in only an apparent dilution of the stronger response from the pure $+\beta$ chromophore thin films. It is interesting to consider what drives the phase separation of the two chromophores on the solid support. One possibility is that electrostatic interactions drive phase separation of the two chromophores, such that self-association of molecules results in structures that are more electrostatically neutral. If this is the case, then it is plausible that choosing $+\beta$ and $-\beta$ chromophores with more closely matched dipole moments may reduce the tendency for unfavorable self-association of the chromophores, and may also enhance film stability.

Cross-linking of layer-by-layer assemble films is a promising strategy for the long-term retention of NLO activity. One approach used by developed by Marks and co-workers employs silane chemistry to generate highly cross-linked and stable chromophore film structures.[16,17,19] LB deposition of chromophores anchored to a polymer backbone, or cross-linking of LB films after deposition are also possible approaches for generating stable films.[45,50,51] Each of these approaches has advantages. Solution phase assembly methods are more applicable for batch preparations and do not require LB instrumentation, whereas LB deposition can take advantage of the specific and rapid self-assembly that occurs at the air/water interface.

While our primary motivation for mixing the $+\beta$ and $-\beta$ chromophores was the opportunity to overcome the electrostatic interactions that are problematic for single chromophore assembly processes,[5,6,49] several other advantages warrant consideration. Substantial investments have been made into designing chromophores with particular shapes[3] or polymers with specific cross-linking functionalities[52] so that high chromophore densities can be achieved with the best possible molecular ordering. Those experiments[7] suggest that a minimal amount of protection (not pursued in these studies) of the chromophores reduces exciton formation. When both $+\beta$ and $-\beta$ chromophore are used, simple rodlike molecules would be expected to have the best performance when they are packed side-by-side in an antiparallel configuration. Another factor that has been considered theoretically, but less so in practice, are local field effects.[53–55] When a single chromophore is loaded into a material at high concentrations and aligned, local field tends to reduce charge separation within the chromophore. The use of two chromophores with similar dipole moments enables local field effects to be minimized. Although layer-by-layer approaches compare unfavorably with poled-polymer films in terms of ease of processing, the potential for generating ultrahigh-β materials with the mixed chromophore method is compelling because of the opportunity to densely pack ordered chromophores in thermodynamically stable configurations.

Acknowledgment. M.H. acknowledges travel support from the UW MDITR STC Postdoctoral Travel Grant. S.L.K. acknowledges support from the NSF (CAREER MCB-0133484). B.H.R. acknowledges support from the NSF (STC-MDITR DMR-0120967). G.J.S. acknowledges support from the Beckman Foundation, the Research Corporation, the Sloan Foundation, and the NSF (CHE-0316177). D.C.C.'s contribution is based on work supported by the Air Force Office of Scientific Research, and the National Science Foundation DMR 0449422, awarded to David Ginger. We thank Phil Reid for use of his 100× objective and for discussions.

CM702267Z

(50) Ulman, A. *An Introduction to Ultrathin Organic Films: From Langmuir-Blodgett to Self-Assembly*; Academic Press: San Diego, CA, 1991.
(51) Esker, A. R.; Mengel, C.; Wegner, G. *Science* **1998**, *280* (5365), 892–895.
(52) Luo, J. D.; Haller, M.; Ma, H.; Liu, S.; Kim, T. D.; Tian, Y. Q.; Chen, B. Q.; Jang, S. H.; Dalton, L. R.; Jen, A. K. Y. *J. Phys. Chem. B* **2004**, *108* (25), 8523–8530.
(53) Bagchi, A.; Barrera, R. G.; Dasgupta, B. B. *Phys. Rev. Lett.* **1980**, *44* (22), 1475–1478.
(54) Bagchi, A.; Barrera, R. G.; Fuchs, R. *Phys. Rev. B* **1982**, *25* (12), 7086–7096.
(55) Ye, P. X.; Shen, Y. R. *Phys. Rev. B* **1983**, *28* (8), 4288–4294.